Supporting Information

Braiterman et al. 10.1073/pnas.1314161111

SI Methods

Subjects and Clinical Laboratory Tests. Normal subjects (Table 1) were healthy volunteers of mean age 35.6 ± 10.5 y, provided informed consent, and were recruited from outpatient clinics and hospital staff from the Medical University of Warsaw. Each volunteer had no family history of Wilson disease (WD), liver disease, or a diagnosed neurodegenerative disease. Individuals with chronic inflammatory disease or infectious disease were excluded. All normal individuals were evaluated and found to lack six WD mutations prevalent in the Polish population. The protocols for the human study group were approved by the Bioethics Committee of the Institute of Psychiatry and Neurology.

Serum ceruloplasmin concentration was measured using p-phenylenediamine as the substrate (1). Serum copper concentration was determined by atomic adsorption spectroscopy. All biochemical investigations were performed at the same laboratory according to the same standardized procedures as previously reported (2, 3).

ATP7B Mutants. Generation of the full-length wild-type ATP7B N-terminally tagged with the green fluorescent protein (wtGFP) ATP7B (designated pYG7) in pAdLOX for adenovirus-mediated protein expression was described previously (4). QuikChange II XL Site-Directed Mutagenesis kit (Stratagene) was used with pYG7 as a template to create GFP-tagged mutants encoded by the plasmids designated pTZs 8R, 13g, 12R, and 21 (Table S2). The ^{858}TGE^{860}>AAA substitution in the A-domain was generated as a negative control (pYG85) for tyrosinase activation. The ORF of GFP was modified in wild-type (wtGFP) ATP7B to generate its monomeric form, A206K (5). The corresponding plasmid, pLB1080, was used as a template to create GFP-tagged mutants encoded by the plasmids AbM18, pTZs 17 and 25, pTuS46, and pAmrs 5, 24, 8, 23, 27, 36, and 37 (Table S2). All primers were from Integrated DNA Technologies (Table S2). Sequences of all mutated regions in each construct were verified.

All constructs were packaged into adenoviruses and purified as described previously (6). To verify that packaged viruses encoded the desired substitutions, adenoviral DNA was purified from infected HEK293A cells, PCR amplified and sequenced as described (7). The sequencing was performed by The Johns Hopkins University DNA Sequencing Facility.

Cell Culture and Adenoviral Infection. Two immortalized derivatives of Simian virus 40 (SV40)-transformed ATP7A-null cells (Menkes fibroblasts), designated YS and YST, were cultured as previously described (4, 8). For protein expression, YS cells were seeded in 10-cm tissue culture dishes containing six glass coverslips (22 × 22 mm); plating densities were either 1.5×10^6 or 7.5×10^5. Cells on coverslips were infected 2 or 3 d later, as described previously (7). WIF-B cells were seeded in 10-cm tissue culture dishes containing six glass coverslips (22 × 22 mm); plating densities were 7×10^5, cultured as described previously (9, 10) and used ∼9–12 d later, when maximal polarity was achieved. WIF-B cells were infected as previously described (8) with the following modifications. Aggregates of virus were removed using 0.2 mm MILLEX GP filter units (Merck Millipore), infections were carried for 0.5 h and the infected cells were cultured overnight with 10 μM bathocuproinedisulfonic acid (BCS). For each recombinant virus, expression of GFP-ATP7B was tested in YS cells as described previously (7).

Tyrosinase Activation and Protein Expression. Each ATP7B construct was tested for its Cu(I) transport activity in YST cells cotransfected with the construct and apo-tyrosinase, then assayed 24 h later as previously described (4, 8). Adenovirus-infected YS cell extracts for protein expression and steady-state half-life studies were harvested and processed as previously described (4, 7).

Indirect Immunofluorescence, Imaging, and Quantification (11). Primary antibodies were obtained from the following sources: mouse anti-TGN38, BD Biosciences; mouse anti-GFP, Clontech; and rabbit antiaminopeptidase N (APN #1637) (12). Secondary antibodies conjugated to Alexa 568 or 647 were from Invitrogen; those with Cy5 were from Jackson ImmunoResearch Laboratories. Immunolabeled WIF-B cells were analyzed using a 100× PLAN-APO, 1.4 NA oil-immersion objective on an LSM 510 META confocal microscope (Zeiss) or using a 40× PLAN-APO, 1.4 NA oil-immersion objective on a Zeiss Axiovert 200 M fluorescence microscope (Zeiss). For imaging, cells that expressed low levels of exogenous protein were selected. The distribution of the GFP-ATP7B variants was assessed relative to the organelle marker, TGN38. Apical surfaces were identified by the presence of either the apical marker, APN, or the phase-lucent circle corresponding to the biliary space in WIF-B cells. Experiments were repeated two or more times and confocal images of 8–20 cells evaluated per experiment. Images of 19–185 cells were acquired using Volocity software (Perkin-Elmer). The response to copper treatment was quantified by counting the total number of polar cells expressing GFP-ATP7B protein, those with ATP7B protein at the apical or basolateral surface (depending on the mutant ATP7B being expressed), and calculating the percent of the total with surface labeling.

Adaptive Poisson–Boltzmann Surface Calculations. The adaptive Poisson–Boltzmann surface (APBS) calculations (Fig. S4) were performed using the APBS Tools2 plug-in (13) within PyMOL. PDB2PQR (14) was used to convert the coordinate file system to PQR format using the AMBER99 force field (15, 16). The calculations performed had dielectric constants set to 2.0 (protein) and 78.0 (solvent), ion concentrations to 150 mM (radius of +1 = 2.0 and −1 = 1.8), probe radius to 1.4 Å and a system temperature of 310 K.

1. Ravin HA (1961) An improved colorimetric enzymatic assay of ceruloplasmin. *J Lab Clin Med* 58:161–168.
2. Gromadzka G, et al. (2005) Frameshift and nonsense mutations in the gene for ATPase7B are associated with severe impairment of copper metabolism and with an early clinical manifestation of Wilson's disease. *Clin Genet* 68(6):524–532.
3. Gromadzka G, et al. (2006) p.H1069Q mutation in ATP7B and biochemical parameters of copper metabolism and clinical manifestation of Wilson's disease. *Mov Disord* 21(2):245–248.
4. Guo Y, Nyasae L, Braiterman LT, Hubbard AL (2005) NH2-terminal signals in ATP7B Cu-ATPase mediate its Cu-dependent anterograde traffic in polarized hepatic cells. *Am J Physiol Gastrointest Liver Physiol* 289(5):G904–G916.
5. Zacharias DA, Violin JD, Newton AC, Tsien RY (2002) Partitioning of lipid-modified monomeric GFPs into membrane microdomains of live cells. *Science* 296(5569):913–916.
6. Bastaki M, Braiterman LT, Johns DC, Chen YH, Hubbard AL (2002) Absence of direct delivery for single transmembrane apical proteins or their "Secretory" forms in polarized hepatic cells. *Mol Biol Cell* 13(1):225–237.
7. Braiterman L, Nyasae L, Leves F, Hubbard AL (2011) Critical roles for the COOH terminus of the Cu-ATPase ATP7B in protein stability, *trans*-Golgi network retention, copper sensing, and retrograde trafficking. *Am J Physiol Gastrointest Liver Physiol* 301(1):G69–G81.
8. Braiterman L, et al. (2009) Apical targeting and Golgi retention signals reside within a 9-amino acid sequence in the copper-ATPase, ATP7B. *Am J Physiol Gastrointest Liver Physiol* 296(2):G433–G444.

9. Cassio D, Hamon-Benais C, Guérin M, Lecoq O (1991) Hybrid cell lines constitute a potential reservoir of polarized cells: Isolation and study of highly differentiated hepatoma-derived hybrid cells able to form functional bile canaliculi in vitro. *J Cell Biol* 115(5):1397–1408.
10. Ihrke G, et al. (1993) WIF-B cells: An in vitro model for studies of hepatocyte polarity. *J Cell Biol* 123(6 Pt 2):1761–1775.
11. Ihrke G, et al. (1998) Apical plasma membrane proteins and endolyn-78 travel through a subapical compartment in polarized WIF-B hepatocytes. *J Cell Biol* 141(1):115–133.
12. Barr VA, Hubbard AL (1993) Newly synthesized hepatocyte plasma membrane proteins are transported in transcytotic vesicles in the bile duct-ligated rat. *Gastroenterology* 105 (2):554–571.
13. Baker NA, Sept D, Joseph S, Holst MJ, McCammon JA (2001) Electrostatics of nanosystems: Application to microtubules and the ribosome. *Proc Natl Acad Sci USA* 98(18):10037–10041.
14. Dolinsky TJ, Nielsen JE, McCammon JA, Baker NA (2004) PDB2PQR: An automated pipeline for the setup of Poisson-Boltzmann electrostatics calculations. *Nucleic Acids Res* 32(Web Server issue):W665–W667.
15. Sorin EJ, Pande VS (2005) Exploring the helix-coil transition via all-atom equilibrium ensemble simulations. *Biophys J* 88(4):2472–2493.
16. DePaul AJ, Thompson EJ, Patel SS, Haldeman K, Sorin EJ (2010) Equilibrium conformational dynamics in an RNA tetraloop from massively parallel molecular dynamics. *Nucleic Acids Res* 38(14):4856–4867.

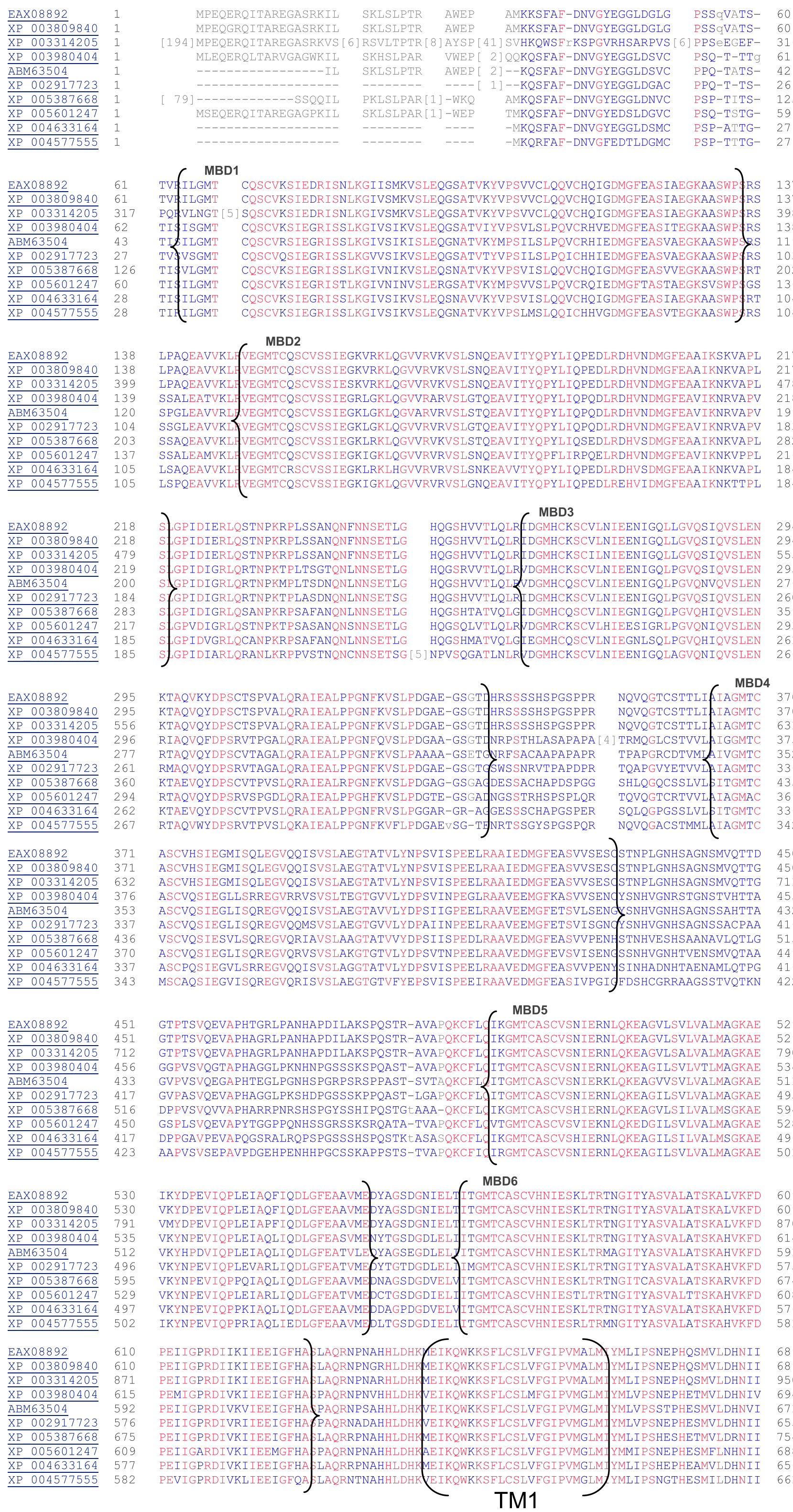

Fig. S1. A multiple species sequence alignment of the N-terminal regulatory domain of ATP7B. Species are EAX08892: human; XP_003809840: pigmy chimpanzee; XP_003314205: chimpanzee; XP_003980404: domestic cat; ABM63504: dog; XP_002917723: giant panda; XP_005387668: long-tailed chinchilla; XP_005601247: horse; XP_004633164: degus rodent; XP_004577555: American pika, rabbit family. Identical amino acids are in red. The sequence before the left bracket shows the linker region for each of the metal binding motifs. Note that the regions linking one metal domain (of ~70 aa) to the next are more divergent (indicated in blue) than the region linking metal binding domain 6 (MBD6) to transmembrane segment 1 (TM1; indicated by closed brackets).

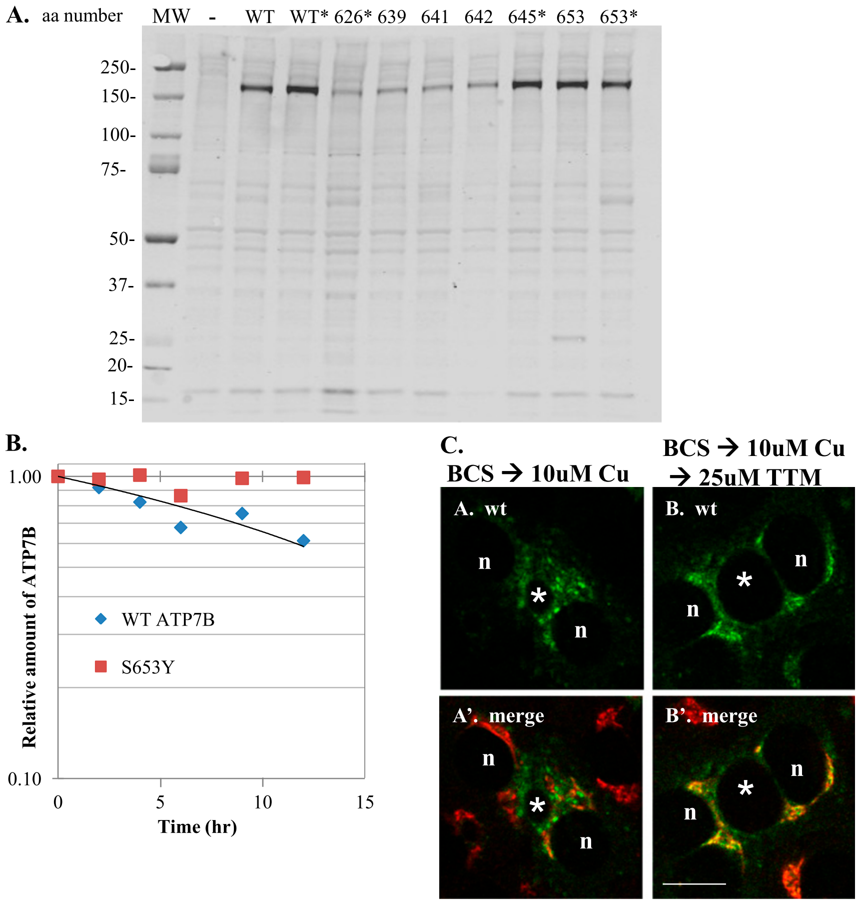

Fig. S2. All 6 ATP7B mutants exhibit Cu(I) transport activity and normal protein characteristics. (*A* and *B*) YS cells on coverslips were infected with the indicated GFP-ATP7B adenovirus, cultured overnight in basal medium, and harvested into urea sample buffer. Denatured proteins were separated by SDS/PAGE, proteins transferred to nitrocellulose, and probed with polyclonal antibody against GFP to show full-length proteins. An asterisk designates the constructs encoding the monomeric version of GFP. In *B*, the relative amount of wt and S653Y ATP7B remaining after the addition of cycloheximide (90 μg/mL) is shown. (*C*) wtATP7B shows normal anterograde and retrograde trafficking. WIF-B cells were infected with wtATP7B, cultured overnight in 10 μM BCS, then incubated in 10 μM $CuCl_2$ for 1 h. One set (anterograde) was fixed and the other set (retrograde) switched to 25 μM ammonium tetrathiomolybdate (TTM) for an additional 2 h before fixation. Cells were stained with anti-TGN and imaged. (*A* and *A*′) In the presence of copper, GFP fluorescence shows no overlap with the TGN marker, whereas after copper chelation (*B* and *B*′) the two signals show strong overlap. (Scale bar, 10 μm.)

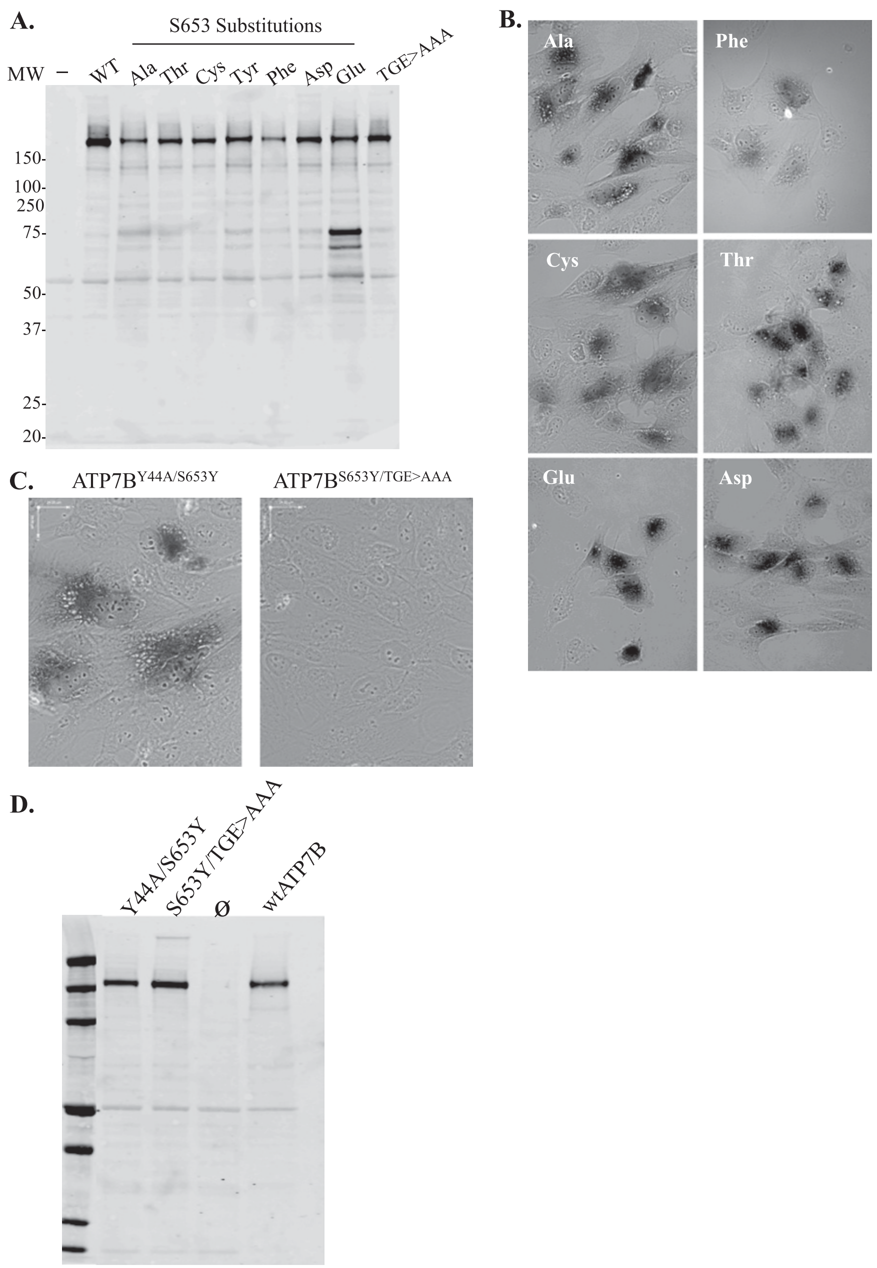

Fig. S3. Recombinant adenoviruses encoding 653 substitutions express full-length ATP7B proteins and exhibit cell-based catalytic activity. (*A*) YS cells infected with the indicated ATP7B adenovirus encoding the designated 653 substitution were processed as in Fig. S1. All constructs expressed full-length proteins except for ATP7BS653E, where proteolytic GFP fragments were routinely observed. (*B*) Each of the 653 substitutions in ATP7B activated tyrosinase as indicated by a black reaction product. (*C*) ATP7B S653Y/Y44A activated tyrosinase, as indicated by a black reaction product, whereas the GFP-ATP7B 858TGE860>AAA/Y44A double-mutant did not. Negative and positive controls were performed in parallel. (*D*) Cell extracts from YS cells infected with GFP-ATP7B adenoviruses encoding the second site mutations were processed as described in Fig. S2. (Magnification: *B* and *C*, 40×.)

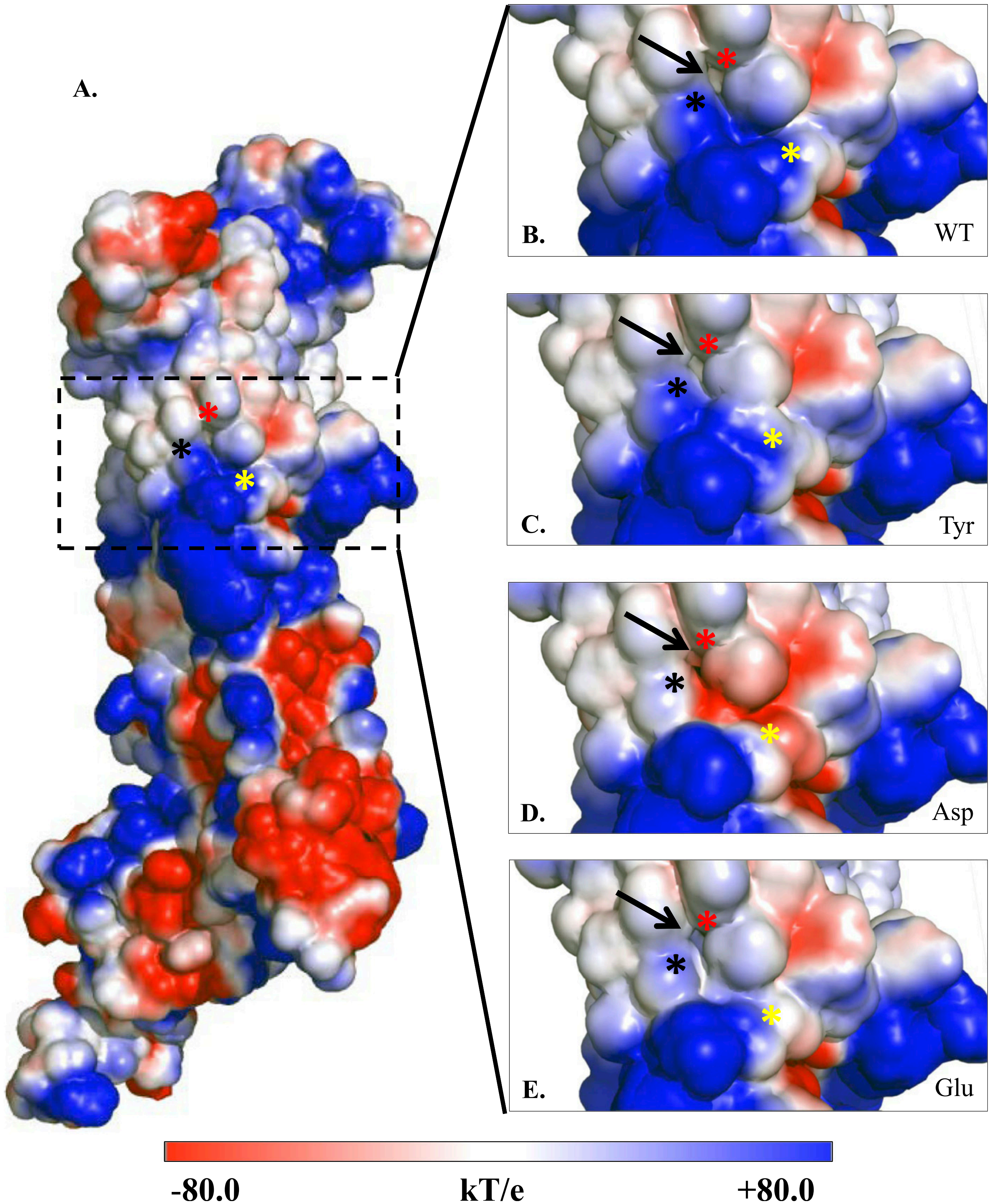

Fig. S4. APBS analysis reveals a pocket (black arrow) near Ser653. (*A*) APBS coloring of the wtATP7B static structure electrostatic potential was calculated according to Poisson–Boltzmann (1). The coloring (red, negative charge; blue, positive charge) range is: $k_BT/e = -80$ to +80. APBS calculations were performed using the APBS tools2 plug-in as part of PyMOL. The boxed region highlights the region near Ser653 and Tyr713. (*B*) An expanded view of *A* shows the surface coloring with the residues of interest highlighted as colored asterisks: black (Ser653, Cα is ~2 Å from the surface), red (Gly710, Cα is ~4 Å from the surface), and

Legend continued on following page

yellow (Tyr713, Cα is ∼1–2 Å from surface). (*C–E*) Expanded views of the Tyr653 (*C*), Asp653 (*D*), and Glu653 (*E*) models show changes in the exposure of positive and negative surface charges within the vicinity of the pocket (black arrow). Notice the predominance of red color (negative charge) in *D*, indicating the effect of charged side chains on the surface charges.

1. Baker NA, Sept D, Joseph S, Holst MJ, McCammon JA (2001) Electrostatics of nanosystems: Application to microtubules and the ribosome. *Proc Natl Acad Sci USA* 98(18):10037–10041.

Table S1. Summary of ATP7B missense mutations found in the conserved region

ATP7B mutation identification (source)	WD mutations in second allele (source)	WD phenotype*	SIFT score designation†	Reported disease-causing status and other findings (source)	Conclusion of this report
G626A (1, 2)	Y187Ifs; Q457X; H1069Q (2)	H; late onset H/N	Deleterious	Inconclusive (3) reduced Cu transport activity (4)	Disease-causing mutation
H639Y‡ (5)	None detected		Deleterious		Inconclusive
L641S (6, 7)			Tolerated		Inconclusive
D642H (6, 8–10)	Homozygous (10)	N; CLF(TX)	Tolerated	Inconclusive (3)	Disease-causing mutation
M645R (11, 12)	Q111X; S932X; N932X; G869R; T977M; H1069Q; V1216M; T132P (12)	H	Tolerated	Increased catalytic phosphorylation likely because of decreased de-phsophorylation activity (4)	Disease-causing mutation
S653Y (5)	H1069Q (Table 1 and ref. 5)	H/N	Deleterious		Disease-causing mutation

CLF, chronic liver failure; H, hepatic; N, neurological; TX, liver transplant.

*Phenotypes reported represent the range observed in the references cited.

†SIFT, a sequence homology based program which sorts intolerant from tolerant substitutions and then classifies them as tolerated or deleterious (13). This analysis is from The Roche Cancer Center Genome Database [see http://rcgdb.bioinf.uni-sb.de/MutomeWeb (14)].

‡Laboratory studies revealed this individual had an unusual presentation of disrupted copper metabolism. The urine copper levels were normal, whereas both ceruloplasmin and serum copper levels were abnormally low, 2.46 mg/dL and 9.0 μg/dL, respectively, as was ^{64}Cu incorporation into ceruloplasmin, which was reduced 10-fold.

1. Figus A, et al. (1995) Molecular pathology and haplotype analysis of Wilson disease in mediterranean populations. *Am J Hum Genet* 57:1318–1324.
2. Todorov T, et al. (2005) Spectrum of mutations in the Wilson disease gene (ATP7B) in the Bulgarian population. *Clin Genet* 68:474–476.
3. Hsi G, et al. (2008) Sequence variation in the ATP-binding domain of the Wilson disease transporter, ATP7B, affects copper transport in a yeast model system. *Hum Mutat* 29:491–501.
4. Huster D, et al. (2012) Diverse functional properties of Wilson disease ATP7B variants. *Gastroenterology* 142:947–956.
5. Gromadzka G, et al. (2005) Frameshift and nonsense mutations in the gene for ATPase7B are associated with severe impairment of copper metabolism and with an early clinical manifestation of Wilson's disease. *Clin Genet* 68(6):524–532.
6. Vrabelova S, Letocha O, Borsky M, Kozak L (2005) Mutation analysis of the ATP7B gene and genotype/phenotype correlation in 227 patients with Wilson disease. *Mol Genet Metab* 86:277–285.
7. Cox DW, Prat L, Walshe JM, Heathcote J, Gaffney D (2005) Twenty-four novel mutations in Wilson disease patients of predominantly European ancestry. *Hum Mutat* 26:280.
8. Loudianos G, et al. (1996) Wilson disease mutations associated with uncommon haplotypes in Mediterranean patients. *Hum Genet* 98:640–642.
9. Zali N, et al. (2011) Prevalence of ATP7B gene mutations in Iranian patients with Wilson disease. *Hepat Mon* 11:890–894.
10. Moller LB, et al. (2011) Clinical presentation and mutations in Danish patients with Wilson disease. *Eur J Hum Genet* 19:935–941.
11. Shah AB, et al. (1997) Identification and analysis of mutations in the Wilson disease gene (ATP7B): Population frequencies, genotype-phenotype correlation, and functional analyses. *Am J Hum Genet* 61:317–328.
12. Margarit E, et al. (2005) Mutation analysis of Wilson disease in the Spanish population–identification of a prevalent substitution and eight novel mutations in the ATP7B gene. *Clin Genet* 68:61–68.
13. Ng PC, Henikoff S (2001) Predicting deleterious amino acid substitutions. *Genome Res* 11:863–874.
14. Kuntzer J, Maisel D, Lenhof HP, Klostermann S, Burtscher H (2011) The Roche Cancer Genome Database 2.0. *BMC Med Genomics* 4:43.

Table S2. Construct summary

Construct	Designation	ATP7B nucleotide change	Mutagenesis primers
Wild-type GFP-ATP7B*	pYG7	None	None
Wild-type mGFP-ATP7B*[†]	pLB1080	None	F-CAGTCCAAGCTGAGCAAAGACCCCAACGAGAA R-GTGATCGCGCTTCTCGTTGGGGTCTTTGCT
ATP7B Patient missense substitutions			
G626A[‡]	pAbM18	G1877C	F-CAAAATTATTGAGGAAATTGCCTTTCATGCTTCCCTGGCCC R-GGGCCAGGGAAGCATGAAAGGCAATTTCCTCAATAATTTTG
H639Y	pTZ13g	C1915T	F- GAAACCCCAACGCTTATCACTTGGACCACAAG R- CTTGTGGTCCAAGTGATAAGCGTTGGGGTTTC
L641S	pTZ8R	T1921C	F-CAACGCTCATCACTCGGACCACAAGATGG R-CCATCTTGTGGTCCGAGTGATGAGCGTTGGG
D642H	pTZ21	G1924C	F-CCCCAACGCTCATCACTTGCACCACAAGATGGAAATAAAG R-CTTTATTTCCATCTTGTGGTGCAAGTGATGAGCGTTGGGG
M645R[‡]	pTZ17	T1934G	F-CATCACTTGGACCACAAGAGGGAAATAAAGCAGTGGAAG R-CTTCCACTGCTTTATTTCCCTCTTGTGGTCCAAGTGATG
S653Y	pTZ12R	C1958A	F- GCAGTGGAAGAAGTATTTCCTGTGCAGCCTGGTG R- CACCAGGCTGCACAGGAAATACTTCTTCCACTGC
S653Y[‡]	pTZ25	C1958A	F- GCAGTGGAAGAAGTATTTCCTGTGCAGCCTGGTG R- CACCAGGCTGCACAGGAAATACTTCTTCCACTGC
Engineered mutations			
S653A[‡]	pAmr8	T1957G T1959C	F- GAAATAAAGCAGTGGAAGAAGGCCTTCCTGTGCAGCCTGGTGTTTGGC R- GCCAAACACCAGGCTGCACAGGAAGGCCTTCTTCCACTGCTTTATTTC
S653F[‡]	pAmr5	C1958T T1959C	F- AAATAAAGCAGTGGAAGAAGTTCTTCCTGTGCAGCCTGGTGTTTGGC R-GCCAAACACCAGGCTGCACAGGAAGAACTTCTTCCACTGCTTTATTTC
S653T[‡]	pAmr23	T1957A	F- GAAATAAAGCAGTGGAAGAAGACTTTCCTGTGCAGCCTGGTGTTTGGC R- GCCAAACACCAGGCTGCACAGGAAAGTCTTCTTCCACTGCTTTATTTC
S653C[‡]	pAmr27	C1958G T1959C	F- GAAATAAAGCAGTGGAAGAAGTGCTTCCTGTGCAGCCTGGTGTTTGGC R- GCCAAACACCAGGCTGCACAGGAAGCACTTCTTCCACTGCTTTATTTC
S653D[‡]	pAmr24	T1957G C1958A	F- GAAATAAAGCAGTGGAAGAAGGATTTCCTGTGCAGCCTGGTGTTTGGC R- GCCAAACACCAGGCTGCACAGGAAATCCTTCTTCCACTGCTTTATTTC
S653E[‡]	pTus46	1957–1959 TCT > GAG	F-GGAAATAAAGCAGTGGAAGAAGGAGTTCCTGTGCAGCCTGGTGTTTGGC R- CCAAACACCAGGCTGCACAGGAACTCCTTCTTCCACTGCTTTATTTCC
Y44A/S653Y[§]	pAmr36	C1958A	F- GCAGTGGAAGAAGTATTTCCTGTGCAGCCTGGTG R- CACCAGGCTGCACAGGAAATACTTCTTCCACTGC
S653Y/TGE > AAA[¶]	pAmr37	C1958A	F- GCAGTGGAAGAAGTATTTCCTGTGCAGCCTGGTG R- CACCAGGCTGCACAGGAAATACTTCTTCCACTGC

Sequences provided upon request.

*Nucleotide numbering corresponds to "A" of ATG as nucleotide +1 of ATP7B in LB1080 and YG7 and encode NM_000053.3 except for the polymorphisms S406A, V456L, R952K, and V1140A (1).

[†]Residue A206 of GFP changed to K to give monomeric GFP (2).

[‡]pLB1080 used as the template for mutagenesis, pYG7 was the template used for all other constructs.

[§]pLB1033 was used as the template for mutagenesis (3).

[¶]pYG85 was used as the template for mutagenesis (*Methods*).

1. Thomas GR, Forbes JR, Roberts EA, Walshe JM, Cox DW (1995) The Wilson disease gene: Spectrum of mutations and their consequences. *Nat Genet* 9:210–217.
2. Zacharias DA, Violin JD, Newton AC, Tsien RY (2002) Partitioning of lipid-modified monomeric GFPs into membrane microdomains of live cells. *Science* 296(5569):913–916.
3. Braiterman L, et al. (2009) Apical targeting and Golgi retention signals reside within a 9-amino acid sequence in the copper-ATPase, ATP7B. *Am J Physiol Gastrointest Liver Physiol* 296(2):G433–G444.